

Modeling of Solid Oxide Fuel Cell with Internal Reforming Operation Fueled by Natural Gas

F. Priyakorn^{1,3}, N. Laosiripojana^{1,3,*}, S. Assabumrungrat²

¹The Joint Graduate School of Energy and Environment, King Mongkut's University of Technology Thonburi, Bangkok, 10140, Thailand

²Center of Excellence on Catalysis and Catalytic Reaction Engineering,

Department of Chemical Engineering, Chulalongkorn University, Bangkok 10330, Thailand

³Centre of Energy Technology and Environment, Ministry of Education, Thailand

*Corresponding author: navadol_l@jgsee.kmutt.ac.th

Abstract: Mathematical models of indirect internal reforming solid oxide fuel cells (IIR-SOFC) fueled by natural gas were developed to analyze the thermal coupling of an internal reformer with electrochemical reactions and to investigate the system performance. The models are based on steady-state, heterogeneous, two-dimensional reformer and annular design SOFC models. The configuration of the internal reformer was considered as conventional packed-bed reactor. The simulations indicated that natural gas is rapidly consumed at the reformer; hence, it appears that the temperature is drops substantially at the entrance of the reformer. It is also observed that the composition of natural gas also plays an important role on the IIR-SOFC thermal and electrical performance. Natural gas from the Gulf of Thailand, after processing, has a lower hydrocarbon content and provides a smoother temperature gradient along the SOFC system, but achieves lower power density and electrical efficiency when compared with natural gas from the North Sea.

Keywords: SOFC; internal reforming; natural gas

1. Introduction

One of advantage of an internal reforming solid oxide fuel cell (IR-SOFC) is it can be used with Hydrocarbon fuels (e.g. methane) as primary fuels. The over all operation is about the utilization of heat from the exothermic electrochemical reaction to the endothermic reforming of hydrocarbons [1-2]. Theoretically, there are two main types of IR-SOFC i.e. direct internal reforming (DIR-SOFC) and indirect internal reforming (IIR-SOFC). For DIR-SOFC, the electrochemical reaction and the reforming reaction occur at the anode side of SOFC. A high heat transfer rate can be achieved from this operation. However, anode material must be optimized for both reactions and could be easily poisoned by carbon deposition from the reforming reaction. As for IIR-SOFC, the endothermic reforming reaction takes place at the reformer, which is in close thermal contact with the anode side of the SOFC where exothermic electrochemical reactions occur. It provides good heat transfer between the reformer and fuel cell and prevents anode material from carbon deposition. Nevertheless, the main drawback of IIR-SOFC is possibly mismatched between rates of endothermic and exothermic reactions, which lead to significant local temperature reductions near the entrance of the reformer. This could result in the mechanical failure due to thermal-induced stresses [3-4]. The operation of the IIR-SOFC generally requires an intensive coupling operation of both the reforming and SOFC.

One hydrocarbon fuel that could be used in an IIR-SOFC is natural gas, the major component of which is methane but includes ethane, propane and some impurities (e.g. water, CO₂, sulfur). Nowadays, many researchers have developed various technologies for utilizing natural gas as a primary feedstock for hydrogen production. Generally, in order to produce hydrogen from natural gas it needs to be purified first. After purification natural gas can be converted into hydrogen by several methods such as, catalytic steam reforming, autothermal reforming, pyrolysis or partial oxidation. Recently, due to the high content of methane in natural gas, it has been proposed as being a suitable feed stock for hydrogen production rather than other hydrocarbons (e.g. methanol, ethanol, biomass, and oil). However, the composition of natural gas is not stable. High methane content natural gas is usually found around the North

side reservoir of Middle East. While the natural gas from south-east Asia has low- methane natural gas. The composition of natural gas could effect the hydrogen production.

The above information suggests it would be interesting to study the performance of IIR-SOFC when fed with Natural gas as a primary fuel. The overall process is begins with the primary fuel and steam being introduced through an indirect internal reformer, located in the middle of the SOFC system, where endothermic steam reforming takes place. At the end of this internal reformer, all product gases flow backward through the anode side of the SOFC, where an exothermic electrochemical reaction occurs. Heat generated from the electrochemical reaction and from ohmic losses [during?] operation is consumed by a reforming reaction and is expected to provide autothermal reaction. Typically, the internal reformer is designed as a packed-bed configuration consisting of pellet or powder shaped Ni-based, Pt-based or Rh-based catalysts. Previous work on the reactivity toward methane, ethane, propane butane and natural gas steam reforming and the kinetic models of Ni-based and Rh-based catalysts have mostly concentrated on lower C₂ and C₂ kinetics [5-8]. Among them, Schadel et al. (2009) [9] studied the kinetics and the conversions of pure methane, ethane, propane, butane and natural gas steam reforming with Rh catalysts and their equations are used in this study.

In the present work, the modeling of IIR-SOFC fueled by natural gas with packed-bed reformer was performed. The mathematical modeling was developed in order to predict the cell performances and temperature gradients along the cell. The model was developed on COMSOL[®] program in 2-dimension axial. The suitable design and suitable composition of IIR-SOFC fueled by natural gas were identified.

2. Model geometry and equations

The internal reformer in the present work is designed in a packed-bed configuration. Natural gas and steam are converted to hydrogen-rich gas at the internal reformer before being introduced to the fuel channel of the tubular SOFC. Simultaneously, air is fed with the same flow direction through the air channel. All dimensions and physical properties of the SOFC system in the present work, which are summarized in

Table 1, are based on previous reports in the literature. According to its structure, each IIR-SOFC component can be separated into porous media (packed-bed and electrodes) and non-porous media (bulk gas channel). For porous structures, it is the porosity, tortuosity and permeability properties of the material that normally affects the transport behaviors of all gases in the system.

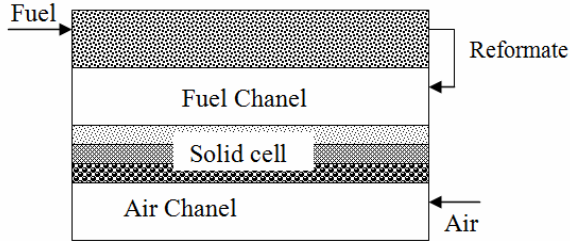


Figure 1. Schematic view of IIR-SOFC with an indirect internal packed-bed reformer in a co-flow direction.

Table 1. Constant parameter values of tubular IIR-SOFC system.

Parameter	Value	Reference
Fuel cell length	0.60 m	[10]
Reformer radius	2×10^{-3} m	[10]
Annular catalyst rod radius	2×10^{-3} m	
Inside radius of the cell	5.4×10^{-3} m	[10]
Anode thickness	1×10^{-3} m	[10]
Electrolyte thickness	4×10^{-5} m	[10]
Cathode thickness	5×10^{-5} m	[10]
Anode permeability	1×10^{-12}	[11]
Cathode permeability	1×10^{-12}	[11]
Average density of triple phase	633.73 kg/m ³	[12]
Average specific heat of triple phase	574.3 J/kg/K	[12]
Anode thermal conductivity	2.7 W/m/K	[12]
Cathode thermal conductivity	9.6 W/m/K	[12]
Convection coefficient in the fuel channel	2987 W/m ² /K	[12]
Convection coefficient in the air channel	1322.8 W/m ² /K	[12]

2.1 Gas distribution

For the gas distribution, Brinkman's equation (1) was applied to calculate the distribution through porous area (packed-bed catalyst and electrodes), while the incompressible Navier-Stokes equation (2) was used to predict gas flow patterns in all gas channels [11].

$$\nabla p = -\frac{\mu}{k_p} \vec{v} + \tilde{\mu} \nabla^2 \vec{v} \quad (1)$$

$$\vec{v} \nabla (\rho \vec{v}) = -\nabla p + \tilde{\mu} \nabla^2 \vec{v} + S \quad (2)$$

where \vec{v} is fluid velocity, ρ is density, p is pressure, $\tilde{\mu}$ is effective viscosity, k_p is permeability, and S is the source term (which is neglected). The pressure and velocity gradient on gas diffusion properties were taken into account by applying molecular diffusion and binary diffusion equations as shown in equations 3 and 4 [13].

$$D_{i,mix} = \frac{(1-y_i)}{\sum_{i,j \neq 1} (y_j / D_{ij})} \quad (3)$$

$$D_{i,j} = \frac{(0.00143) T^{1.75}}{p M_{i,j}^{1/2} [\gamma_i^{1/3} + \gamma_j^{1/3}]^2} \quad (4)$$

where $D_{i,mix}$ and $D_{i,j}$ are molecular diffusion and binary diffusion flux of species i in mixed gas (m²/s), y_i is the mole fraction of species i , p is pressure, $M_{i,j} = 2/(1/M_i + 1/M_j)$ and M_i is the molecular weight of component i , and γ is the special

diffusion volume (reported by Fuller et al. [10]). The diffusion behavior was corrected by applying porosity (ϵ), tortuosity (τ), and effective diffusivity coefficient, $D_{i,pmix}^e$, as shown in equation 5. Furthermore, gas diffusion through porous media, $D_{i,pmix}$, was explained in equation 6 by two mechanisms of molecular diffusion ($D_{i,mix}$) and Knudsen diffusion ($D_{i,ku}$), which depends on the relation between pore diameter (d_p) and mean free path of molecular species (equation 7).

$$D_{i,pmix}^e = \frac{\epsilon}{\tau} D_{i,pmix} \quad (5)$$

$$\frac{1}{D_{i,pmix}} = \frac{1}{D_{i,mix}} + \frac{1}{D_{i,ku}} \quad (6)$$

$$D_{i,ku} = \frac{1}{3} d_p \sqrt{\frac{8RT}{\pi M_i}} \quad (7)$$

2.2 SOFC Model

The electricity generation was calculated from the relation between polarization and the activated area of SOFC. Activation, concentration and ohmic polarization are known to be major losses of potential voltage for high-temperature fuel cells like SOFCs. Activation loss arises from an activation barrier to the electrochemical reaction at the electrode. In this work, the activation polarization, η_{act} , was computed by;

$$J_i = J_0 \left[\exp\left(\frac{\alpha_a F \eta_{act}}{R_g T}\right) - \exp\left(\frac{-(1-\alpha_c) F \eta_{act}}{R_g T}\right) \right] \quad (8)$$

where J_i is the current density (Am⁻²); J_0 is the exchange current density (Am⁻²); R_g is the universal gas constant (kJ mol⁻¹ K⁻¹); And F is the Faraday constant. All relevant parameters were reported by Zhu et al. [10]. The concentration polarization occurs due to the resistance to gas diffusion through the porous media. Generally, gas diffusion behaviour can be predicted by three mathematical models: Fick's model, The Dusty gas model (DGM), and The Stefan-Maxwell model; the DGM was chosen in the present work. Ohmic polarization arises from the ion transport across the cell, which mainly depends on the ionic conductivity of the SOFC material. By applying ohm's law, the relation of ohmic polarization and material resistivity can be determined. In the present work, the material properties reported by Zhu et al. [10] were used. The voltage drop was computed by the simplified equation:

$$\eta_{ohmic} = J R_{ohm} \quad (9)$$

where ohmic is the voltage drop caused by ohmic losses (V); J is the current density (Am⁻²), and R_{ohm} is the ohmic resistant per unit area (kΩm²). Although both H₂ and CO can be electrochemically consumed in a SOFC, it has been widely reported that the rate of electricity generation from CO is three times lower than that of H₂; thus the rate of CO oxidation in the SOFC has been neglected in this study. At the anode|electrolyte interface, H₂ is electrochemically oxidized whereas O₂ is consumed at the cathode|electrolyte interface. The conversion rate of H₂, R_{elec,H_2} , and O₂, R_{elec,O_2} at the indicated boundary was simulated from Equations 10 and 11, respectively:

$$R_{elec,H_2} = \frac{J_{H_2}}{2F} \quad (10)$$

$$R_{elec,O_2} = \frac{J_{O_2}}{4F} \quad (11)$$

The reliability of these electrochemical equations, coded in COMSOL® program, was validated by comparison with the

results from the work of Lin et al. [14]. Clearly, the results are in good agreement.

2.3 Efficiency

Based on the assumption that most of the generated hydrogen was combusted to supply heat for the steam reforming reaction, some heat generated from reformer was used as the heat source. The thermal efficiency, $Eff_{thermal}$, of an IIR-SOFC in this section was defined as the ratio between the heating value of hydrogen left over from combustion with that of the inlet fuel as shown in equation 12

$$Eff_{thermal} = \frac{n_{H_2}^{out} LHV_{H_2,1173K} - \sum (-\Delta H_{reform})}{\sum n_i^{in} LHV_{i,1173K}} \quad (12)$$

where n_i is the number of moles of component i and $LHV_{i,1173K}$ is the lower heating value of component i at 1173 K. In order to investigate the electrical efficiency, the outlet reformates were

fed into the fuel channel of tubular SOFC. The electrical efficiency, Eff_{elec} , was defined in the following equation.

$$Eff_{elec} = \frac{P_{SOFC} \cdot A_{act}}{\sum Y_i^{in} LHV_{i,1173K}} \quad (13)$$

where A_{act} is the active area (m^2) and y_i^{in} is the mole fraction of the inlet fuel.

3. Mass Balance and Energy Balance in the Reformer and SOFC model

Heat transfer in this system involves the conduction along stack materials. Conversion from heat flow through the system and radiation between the reformer and SOFC were concerned [15-16]. Mass and energy balances for the four configurations of internal reformer and SOFC are given in Table 1 and 2, respectively.

Table 2. Steady state 2-D dimensional model for tubular packed bed, coated wall, annular and annular coated wall.

Mass balance	$\nabla(-D_i \nabla c_i + c_i \vec{v}) - \rho_B \sum v_i R_{reform} = 0$	(14)
Energy balance	$\nabla(\vec{v} \rho C_p T) - \nabla(\lambda_i \nabla T) + \sum \Delta H_{reform} R_{reform} = 0$	(15)
Boundary	$z = 0; r \geq 0; u_r = 0, v_r = v_{r,in}, c_{i,r} = c_{i,in}, T_r = T_{r,in}$ $r = r_z; z \geq 0; n \cdot (k \nabla T) = \lambda_{r,f} (T_r - T_f) + \frac{\sigma A_s (T_r^4 - T_s^4)}{\frac{1}{\epsilon_r} + \frac{A_r}{A_s} \left(\frac{1}{\epsilon_s} - 1 \right)}$	

Table 3. Steady state 2-D dimensional model for tubular SOFC.

Fuel channel		
Mass balance	$\nabla(-D_i \nabla c_i + c_i \vec{v}) - \sum v_i R_{elec} = 0$	(16)
Energy balance	$\nabla(\vec{v} \rho C_p T) - \sum \nabla(\lambda_i \nabla T) = 0$	(17)
Boundary	$z = L; r \geq 0; u_f = u_r, v_f = v_r, p_f = p_r, c_{i,f} = c_{i,r}, T_f = T_r$ $r = r_r; z \geq 0; n \cdot N_{H_2,f} = -J_{H_2} / 2F, n \cdot N_{H_2O,f} = J_{H_2} / 2F$ $n \cdot N_{CO,f} = -J_{CO} / 2F, n \cdot N_{CO_2,f} = J_{CO} / 2F$ $n \cdot (k \nabla T) = h_{r,f} (T_f - T_r)$	
Solid cell		
Energy balance	$\nabla(\vec{v} \rho C_p T) - \nabla(\lambda_s \nabla T) + \sum \nabla H_{elec} + \frac{\sigma A_s (T_r^4 - T_s^4)}{\frac{1}{\epsilon_r} + \frac{A_r}{A_s} \left(\frac{1}{\epsilon_s} - 1 \right)} = 0$	(18)
Boundary Anode/electrolyte interface,	$n \cdot (k \nabla T) = \sum \Delta H_{elec} R_{elec} + J \eta_{total}$ $r = r_f; z \geq 0; n \cdot (k \nabla T) = h_{f,s} (T_s - T_f)$ $r = r_s; z \geq 0; n \cdot (k_{sa} \nabla T) = h_{sa} (T_a - T_s)$	
Air channel		
Mass balance	$\nabla(-D_i \nabla c_i + c_i \vec{v}) = 0$	(19)
Energy balance	$\nabla(\vec{v} \rho C_p T) - \sum \nabla(\lambda_i \nabla T) = 0$	(20)
Boundary	$z = 0; r \geq 0; u_a = 0, v_a = v_{a,in}, c_{i,a} = c_{a,in}, T_a = T_{in}$ $r = r_a; z \geq 0; n \cdot N_{O_2,f} = -J_{O_2} / 2F$ $n \cdot (k \nabla T) = \lambda_{f,s} (T_s - T_f)$ $r = r_0; z \geq 0, n \cdot (k \nabla T) = 0$	

4. Results and discussion

4.1 System validation

The model was developed as the smallest single unit cell taking into account the effect of temperature on gas distribution, reactant conversion, and charge transfer. The assumptions made were (i) each section was considered as non-isothermal steady-state conditions; (ii) ideal gas behavior was applied for all gas components; (iii) pressure drops in the SOFC stack and the coated-wall reformer were neglected; and (iv) fuel utilization was fixed constantly at 80% along the length of the cell. A number of equations were applied to predict concentration and temperature gradients along these tubular IIR-SOFC systems. Because the cell parameters are values from the computer model of literature [10-12], we compared the result of voltage and current from the developed model with the experiment data of Lin et al., (2006) [14] in order to ensure that the developed model was reliable. As shown in Fig. 1, the difference between simulation results and experimental results is acceptable.

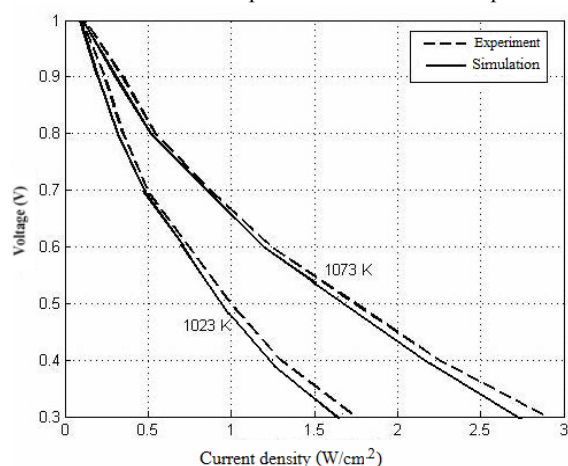


Figure 2. I-V curve validations between the simulation results in the present work with the experimental results from literature (Lin et al., 2006 [14]).

4.2 Modeling of IIR-SOFC fueled by natural gas

IIR-SOFC model was firstly simulated at 1173 K and 1 bar. The mixture of natural gas and steam, with a steam to carbon ratio of 2.0, was introduced to the system. It was noted that the flow rate of inlet fuel applied for all configurations was $12.2 \text{ cm}^3/\text{s}$ whereas the inlet air flow rate to the cathode was $94.24 \text{ cm}^3/\text{s}$ (theoretical ratio). It was noted that the requirement of high air flow rate for internal stack cooling becomes less demanding under IIR-SOFC operation.

In addition, the SOFC load voltage of 0.7 V and a fuel utilization of 80% were applied. Figure 3 shows the concentration profiles of methane, ethane, propane, butane, steam, hydrogen, carbon monoxide, and carbon dioxide in the reformer and fuel channel of the IIR-SOFC system with a packed bed internal reformer.

It can be seen that the amount of all hydrocarbons as well as steam decrease along the length of the reformer, whereas hydrogen, carbon monoxide and carbon dioxide increase. At the end of the reformer, all hydrocarbons are completely converted; and the gaseous product mainly consisted of 75% H_2 , 13% CO , 12% H_2O , and 2% CO_2 . This gaseous product then flows backward to the fuel channel of the SOFC and the electrochemical reaction takes place to generate electricity. It was noted that, from the simulation, the vent gas at the outlet of the fuel channel consisted of 38% H_2 , 8% CO , 40% H_2O , and 14% CO_2 . As the next step, the temperature profiles at the reformer, fuel and air channels of these four IIR-SOFC systems were predicted as

shown in Figures 4 and 5. According to the simulation, it was revealed that the temperature gradient occurred at the entrance of the reformer.

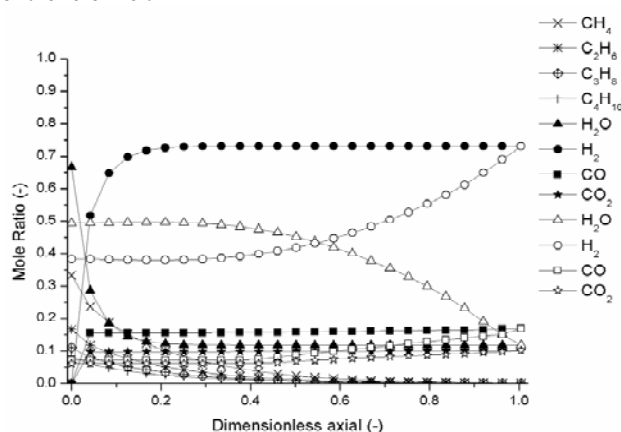


Figure 3 Concentration profile in the reformer (white symbol) and fuel channel (black symbol) of IIR-SOFC with packed – bed reformer.

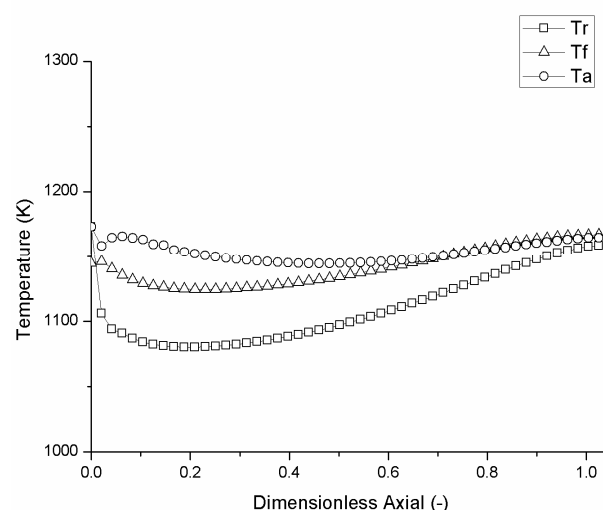


Figure 4. Temperature profile of the reformer (Tr), Temperature profile of fuel channel (Tf) and Temperature profile of air channel (Ta) of IIR-SOFC with packed – bed reformer.

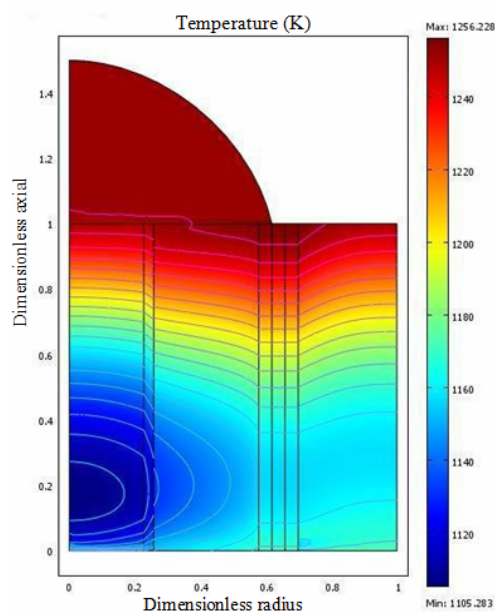


Figure 5. Results from COMSOL[®] represented temperature gradients in the reformer and fuel channel of the IIR-SOFC.

The performances of this IIR-SOFC system were considered in terms of the power density and electrical efficiency. The power density was observed to be 0.53 W/cm^2 , while the electrical efficiency was 41%. In addition, the pressure drop across the IIR-SOFC was predicted to be $2.69 \times 10^{-4} \text{ kPa}$.

4.3 Effect of natural gas composition

In this section, the effect of natural gas composition (hydrocarbon and impurity contents) on the IIR-SOFC performance achievement (in terms of temperature profile, power density and electrical efficiency) was investigated. The composition of natural gas from the base case (from the North Sea) was changed into 2 categories, raw and sale natural gas from the Gulf of Thailand. The compositions of natural gas from these 3 sources are given in Table 4.

The thermodynamic properties of 3 different compositions of natural gas were identified in terms of lower heating value (LHV) and thermal efficiency. According to the thermal efficiency calculation, a steady state operation was assumed and the inlet fuel was kinetically converted to hydrogen in the reformer, which was eventually combusted to predict the thermal efficiency. The simulation was carried out at 1173 K and 1 bar with the inlet steam to carbon (S/C) ratio of 2.0. The LHV value and thermal efficiency of the fuel is shown in Table 5. The LHV and thermal efficiency of pure methane is also given for comparison. Although the LHV values were similar the thermal efficiency of pure methane was highest.

Figure 6 shows the temperature gradients at the reformer, fuel and air channels of the IIR-SOFC fueled by natural gas from different sources; the temperature gradients of the IIR-SOFC fueled by pure methane are also given for comparison. The temperature profiles of all channels (reformer, fuel and air channel) from different compositions in Figure 6 were rather similar. The gradient of temperature profiles at the inlet of reformer were notice. Among them, the IIR-SOFC fueled by pure

methane shows the largest cooling spot at the first half of the reformer channel (temperature drop from 1173 K to 1020 K), whereas the IIR-SOFC fueled by raw and sale natural gas were smoother (reformer temperature decreased from 1173 K to 1071 and 1098, respectively). The temperature of all channels begins accumulated in the middle of the tube for all conditions. From the literature, the temperature gradient along the system can affect the cell performance and the properties of the ceramic components. The temperature difference should not be too high [15]. According to the present analysis, an IIR-SOFC fueled with sale natural gas can meet this criterion. The results of electrical efficiency and power density of each category are shown in Figure 7.

Table 4. Compositions of natural gas in base case, raw and sale natural gas from Thailand gulf.

Content (%vol)	Base case from North Sea	Raw Natural Gas from Thailand Gulf	Sale Natural Gas from Thailand Gulf
CH ₄	87.72	67.39	72.311
C ₂ H ₆	8.44	9.33	7.245
C ₃ H ₈	3.30	5.15	2.192
C ₄ H ₁₀	0.54	2.22	0.93
CO ₂	-	14.26	14.698

Table 5. Thermal properties (LHV and thermal efficiency) and Volumetric flow rate of each fuel under isothermal conditions (1173 K and 1bar).

Composition	LHV (kJ/mol)	Thermal Efficiency (%)	Volumetric Flow rate (cm ³ /s)
Pure Methane	744.7	42	0.15
Base case	798.9	38	0.17
Raw gas	695.2	34	0.20
Sale gas	771.05	35	0.19

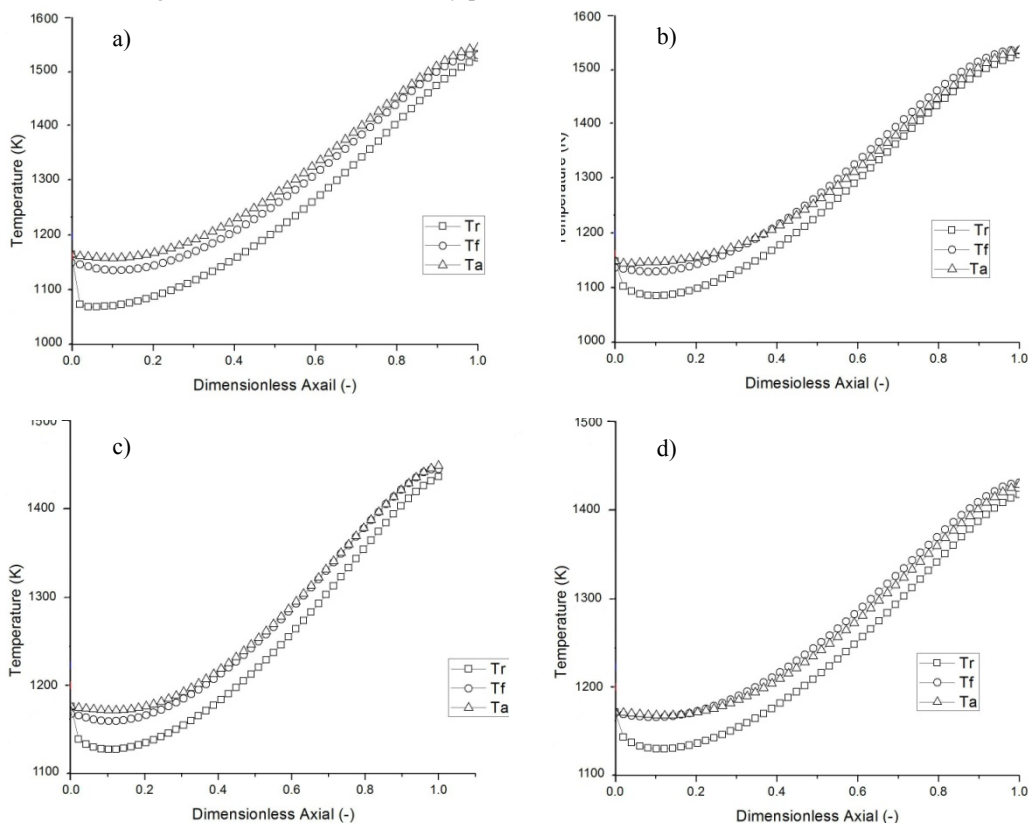


Figure 6. Effect of composition on temperature profile which operated under co-flow pattern at 1173 K, a) pure methane b) natural gas from base case c) raw natural gas from the Gulf of Thailand d) sale natural gas in Thailand.

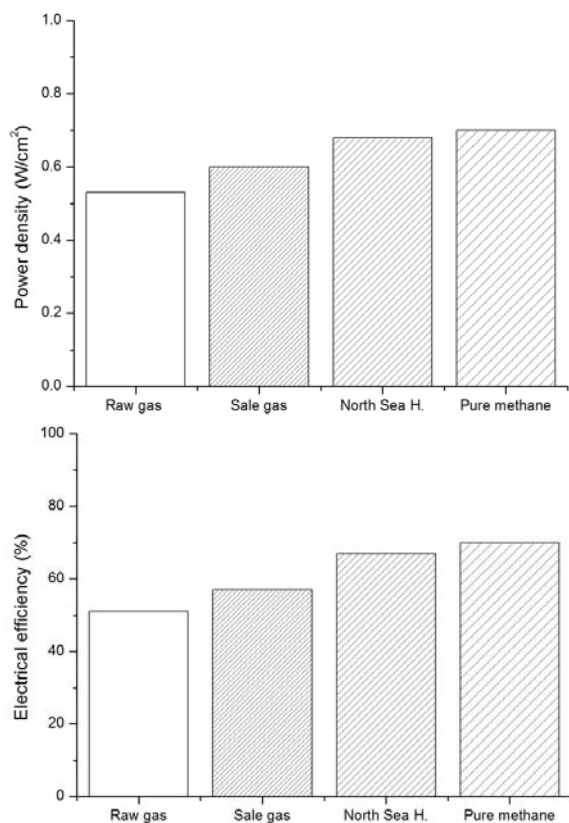


Figure 7. Effect of composition on power density and electrical efficiency achieved from IIR-SOFC with annular coated wall, which operated under co-flow pattern at 1173 K, pure methane, base case, raw gas and sale gas.

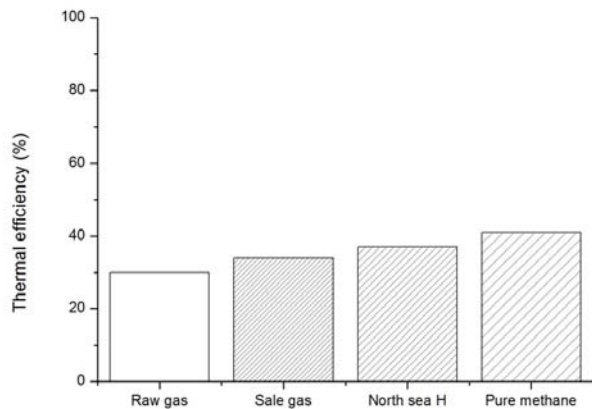


Figure 8. Thermal efficiency of 3 different compositions of natural gas, raw gas, sale gas and north sea H (base case), compared with pure methane under isothermal condition (1173K, 1 bar).

In addition to the temperature distribution, the natural gas composition also affects the power density and electrical efficiency of the system. The power density and electrical efficiency of pure methane and base case are higher than raw and sale natural gas from the Gulf of Thailand. It can be seen from Figure 7 that the power density and electrical efficiency decrease when increasing the CO₂ content of the feed. The lowest electrical efficiency and power density is when feeding with raw natural gas which has a high amount of CO₂ and low amount of CH₄. Although the amount of CO₂ in raw natural gas and sale natural gas is similar, sale natural gas has more 10% of CH₄. The result shows that electrical efficiency and power density of sale natural gas increases by 8% and 56% respectively when compared with raw natural gas. Fuel composition that has high CO₂ (around 15%) can effect the cell voltage could be decreased

to 12% [17]. It is well known that the presence of a high CO₂ [concentration] is a major problem for natural gas in terms of several energy aspects, e.g., combustion for power generation or use as fuel in vehicle.

Lastly, the thermal efficiencies achieved from each feedstock were also calculated as shown in Figure 8. It was also observed that a similar trend as the electrical efficiency and power density was accepted. Raw natural gas provided the lowest thermal efficiency.

5. Conclusion

The simulations of the IIR-SOFC fueled by natural gas with a conventional packed-bed internal reformer indicated that all hydrocarbons in natural gas (i.e. methane, ethane, propane, and butane) were rapidly consumed at the entrance of the reformer. Hence, it appeared that the temperature dropped sharply at the entrance of the reformer, which is mainly related to the mismatch between the rapid endothermic steam reforming reaction rate and the amount of heat supplied from the electrochemical reaction. It was also observed that the composition of natural gas played an important role in the IIR-SOFC thermal and electrical performance. Comparing natural gas from the base case to natural gas in Thailand (i.e. the raw gas from the Gulf of Thailand, and the sale natural gas after processing), Thai natural gas had lower methane content and provided a smoother temperature gradient along the SOFC system, but achieved lower power density and electrical efficiency.

References

- [1] Dicks AL, Hydrogen generation from natural gas for the fuel cell systems of tomorrow, *Journal of Power Sources* 61 12 (1996) 113-124.
- [2] Mauri R, A new application of the reciprocity relations to the study of fluid flows through fixed beds, *J Eng Math* 33 (1998) 103-112.
- [3] Park HK, Lee YR, Kim MH, Chung GY, Nam SW, Hong SA, Lim TH, Lim HC, Studies of the effects of the reforming in an internal-reforming molten carbonate fuel cell by mathematical modeling, *J. of Power Sources* 104 (2002) 140-147.
- [4] Aguiar P, Chadwick D, Kershenbaum L, Effect of methane slippage on an indirect internal reforming solid oxide fuel cell, *Chem. Eng. Sci.* 59 (2004) 87-97.
- [5] Takeguchi T, Kani Y, Yano T, Kikuchi R, Eguchi K, Tsujimoto K, Uchida Y, Ueno A, Omshiki K, Aizawa M, Study on steam reforming of CH₄ and C₂ hydrocarbons and carbon deposition on Ni-YSZ cermets, *J Power Sources* 112 (2002) 588-595.
- [6] Zavarukhin SG, Kuvshinov GG, The kinetic model of formation of nanofibrous carbon from CH₄-H₂ mixture over a high-loaded nickel catalyst with consideration for the catalyst deactivation, *J Applied catalysis* 272 (2004) 219-227.
- [7] Machli M, Boudouris C, Gaab S, Find J, Lemonidou AA, Lercher JA, Kinetic modelling of the gas phase ethane and propane oxidative dehydrogenation, *J Catalysis Today* 112 (2006) 53-59.
- [8] Xu J, Froment GF, Methane steam reforming, methanation and water-gas shift: I intrinsic kinetics, *AIChEj* 35 (1989) 88-96.
- [9] Schadel BT, Duisberg M, Deutschmann O, Steam reforming of methane, ethane, propane, butane, and natural gas over a rhodium-based catalyst, *Catalysis Today* 142 (2009) 42-51.
- [10] Zhu H, Colclasure AM, Kee RJ, Lin Y, Barnett SA, Anode barrier layers for tubular solid-oxide fuel cells with methane fuel streams, *J Power Sources* 161 (2006) 413-419.

- [11] Costamagna P, Selimovic A, Borghi MD, Agnew G, Electrochemical model of the integrated planar solid oxide fuel cell (IP-SOFC), *Chem Eng J* 102 (2004) 61-69.
- [12] Xue X, Tang J, Dynamic modeling of single tubular SOFC combining heat/mass transfer and electrochemical reaction effects, *J. Power Sources* 142/1-2 (2005) 211- 221.
- [13] Fuller EN, Schettler PD, Giddings JC, A new method for prediction of binary gas-phase diffusion coefficients, *Ind Eng Chem* 58 (1996) 19-27.
- [14] Lin Y, Zhan Z, Barnett SA, Improving the stability of direct-methane solid oxide fuel cells using anode barrier layers, *J. Power Sources* 158 (2006) 1313-1316.
- [15] Lutz AE, Bradshaw RW, Keller JO, Witmer DE, Thermodynamic analysis of hydrogen production by steam Reforming, *Int. J. Hydrogen Energy* 28 (2003) 159-167.
- [16] Ni M, Leung DY, Leung MKH, Electrochemical modeling and parametric study of methane fed solid oxide fuel cells, *Energy Conversion and Management* 50 (2009) 268-278.
- [17] Grof E, *Fuel composition effects and other operational parameters on solid oxide fuel cell performance* (2010) National energy technology laboratory, USA.

List of Abbreviations and Symbols

Abbreviations

DIR	Direct internal reforming
EMF	Electo-motive-force
IIR	Indirect internal reforming
IR	Internal reforming
MCFC	Molten carbonate fuel cell
OCP	Open-circuit potential
PEN	Positive electrode/Electrolyte/Negative-electrode
POX	Partial oxidation reaction
RWGS	Reverse water-gas shift reaction
SOFC	Solid oxide fuel cell
WGS	Water gas shift reaction

Symbols

A_{act}	Active surface area = $\frac{\pi(d_r - 2\tau_{cat})L}{\pi(d_r^2 - (d_r - 2\tau_{cat})^2)L}$
A_{anode}	Anode active surface area $2\pi r_f L, m^2$
A_f	Fuel channel outer surface area $2\pi r_f L, m^2$
A_r	Reformer outer surface area $2\pi r_r L, m^2$
A_s	Solid electrolyte outer surface area $2\pi r_s L, m^2$
C_p	Specific heat of the gas streams, kJ/mol/K
c_i	Concentration, mol/m ³
$D_{i,j}$	Binary diffusion, m ² /s
$D_{i,mix}^e$	The effective molecular diffusivity, m ² /s
$D_{i,ku}$	The kundsens diffusivity, m ² /s
d_p	Pore diameter, m
E	EMF or open circuit voltage, Volts
E_{act}	Activation energy, kJ/mol
Eff_{elec}	Electrical efficiency
$Eff_{thermal}$	Thermal efficiency
F	Faraday's constant, 96,487 C/mol
F_{12}	Gray-body transfer factor from surface 1 to surface 2
ΔG_f	The change in Gibbs free energy of formation

Δg_f°	The change in Gibbs free energy of formation per mole(kJ/mole) at STD
ΔH	The change of heat of reaction, kJ/mol
$(-\Delta H)_{elec}$	Heat of the electrochemical reaction, kJ/mol
j_0	Exchange current density, mA/cm ²
j	Current density, mA/ cm ²
j_{H_2}	Current density from hydrogen oxidation reaction, mA/ cm ²
k_i	Rate constant for reaction 'i'; unit will be specific to the form of the rate expression
k_{cond}	Thermal conductivity, W/m ² .K
k_p	Permeability
$LHV_{i,1173K}$	Lower heating value of component i at 1173 K.
N_i^D	The bulk molar diffusive flux of gas component, mol/m.s
n	Number of electron that pass round the external circuit
P_{SOFC}	Power Density, W/m ²
p^0	Standard partial pressure, bar
p_i	Partial pressure of species i ,
q_{rad}	The heat flux from radiation, W/m ²
Q_{gen}	Local generated heat, W/m ²
R_g	Universal gas constant; 8.414 kJ/mol K.
R_c	Rate of nanocarbon fiber formation (g/h.g)
R_{elect}	The hydrogen oxidation reaction rate, mol/m ² s
R_k	Rate of reaction k
R_{ohm}	Ohmic Polarization, Ωm^2
ΔS	The change in Entropy, kJ/mol
S_{act}	Specific surface area of catalyst
T	Temperature, K
U_{eff}	Fuel utilization factor
u	Fluid velocity, m/s
V_{cell}	Voltage drop of the whole cell, Volts
V_{ohmic}	Voltage drop caused by ohmic losses , Volts
y_i	The mole fraction of gas

Greek letters

ρ_B	Catalyst bulk density, kg/m ³
ϵ_m	Emittance
\mathcal{G}	Exchange current density constant, mA/cm ²
$\alpha_{a,c}$	Charge transfer coefficient of anode and cathode
σ	Stefan-Boltzmann coefficient
ϵ	Porosity
τ	Tortuosity
λ	Thermal conductivity (kJ/m/s/K),
δ_{air}	Air Ratio
$\tilde{\mu}$	Effective viscosity, Pa.s
γ	Special Fuuller <i>et.al</i> diffusion volume
Γ	Thickness, m

Subscripts

<i>a</i>	Air channel	<i>Cat</i>	Catalyst
<i>c_{form}</i>	Carbon formation	<i>Cell</i>	Cell stack
<i>i</i>	Component (methanol, water, hydrogen, etc.)	<i>Con</i>	Concentration losses
<i>j</i>	Reaction (SRM, WGS, etc.)	<i>cathode</i>	Cathode
<i>f</i>	Fuel channel	<i>ohm</i>	Ohmic losses
<i>p</i>	Particle	<i>elec</i>	Electrochemical reactions
<i>s</i>	Solid oxide fuel cell	<i>rod</i>	Catalyst Rod
<i>Act</i>	Activation losses	<i>reform</i>	Reforming
<i>anode</i>	Anode	<i>Thermal</i>	Thermal